Preparation and Characterization of Trimethylamine–Alane Thin Films on Oxidized Silicon

Fiona M. Elms,† Robert N. Lamb,‡ Paul J. Pigram,*,‡ Michael G. Gardiner,† Barry J. Wood,§ and Colin L. Raston†

Faculty of Science and Technology, Griffith University, Nathan, Brisbane, Queensland, 4111, Australia; Department of Physical Chemistry, University of New South Wales, Kensington, N.S.W., 2033, Australia; and Brisbane Surface Analysis Facility, University of Queensland, Brisbane, Queensland, 4072, Australia

Received March 2, 1994®

The surface adsorption characteristics of trimethylamine–alane, H_3AlNMe_3, on a SiO_2 substrate have been investigated using X-ray photoelectron spectroscopy and static secondary ion mass spectrometry. Molecular adsorption prevails at exposures of ~15 langmuirs with the aluminum centers becoming five-coordinate *via* binding to surface oxygen centers. High XPS X-ray flux (>240 W) results in migration of NMe_3 to silicon centers, ascertained by comparison with the adsorption of NMe_3 gas. At exposures greater than ~30 langmuirs an aluminum-rich species is formed, with the ratio of Al:N close to 2:1. Similar results are obtained for dosing of bis-(trimethylamine)–alane, $H_3Al(NMe_3)_2$. *Ab initio* molecular orbital calculations (HF/D95*) on H_3AlNH_3 and H_2O, and H_3AlOH_2, as model systems for the interaction of H_3AlNMe_3 with surface oxygen centers, gave formation of $H_3AlNH_3(OH_2)$ as energetically favored by 4.53 kcal mol^{-1} and its fragmentation to H_3AlOH_2 and NH_3 requiring 13.16 kcal mol^{-1}; association of H_3AlOH_2 and H_3AlNH_3 to $H_2(NH_3)Al(\mu\text{-}H)_2Al(OH_2)H_2$, as a model for the aluminum-rich species, is also favored by 3.39 and 3.24 kcal mol^{-1} for two isomers with different orientations of the H atoms on sp^3 oxygen.

Introduction

Aluminum films are important in the field of microelectronics and are usually generated by various chemical vapor deposition (CVD) techniques. In such applications, high quality films can be generated, for example, using triisobutylaluminum (TIBA)[1-3] as the precursor. The growth rate is limited, however, by the decomposition of a surface isobutyl intermediate, derived from the dissociative chemisorption of the precursor *via* β-hydrogen elimination.[2,3] The resulting aluminum hydride species then readily lose hydrogen to give a metal film. Carbon contamination of the film and the formation of rough film surfaces with poor reflective properties also result from the use of this precursor.[1]

One method of eliminating the problems of slow surface kinetics and carbon contamination is to use aluminum hydride precursors such as tertiary amine adducts of alane, for example, H_3AlNMe_3 (TMAA) and $H_3Al(NMe_3)_2$ (BTMAA). These are volatile compounds; the absence of direct metal–carbon interactions avoids carbon incorporation in thin films formed by the decomposition of these compounds. TMAA and BTMAA have been successfully used to prepare thin films of Al using laser-induced chemical vapor deposition (LICVD),[4] low-pressure chemical vapor deposition (LPCVD),[1-3,5] and molecular beam epitaxy (MBE).[6] They have also been used in electroless[7] and electrosolution aluminum plating.[8] Studies of the surface reactivity of these precursors on Si, Al, and GaAs substrates have yielded reactions 1–4.[2,3,6] It has been reported that

$$H_3AlNMe_3(g) \rightarrow H_3AlNMe_3(ads) \quad (T = 150\ K) \quad (1)$$

$$H_3AlNMe_3(ads) \rightarrow AlH_3(ads) + NMe_3(g) \quad (T = 200\text{–}400\ K) \quad (2)$$

$$AlH_3(ads) \rightarrow Al(m) + H_2(g) + H(ads) \quad (T = 500\ K) \quad (3)$$

$$2H(ads) \rightarrow H_2(g) \quad (T = 600\ K) \quad (4)$$

BTMAA adsorbs molecularly on GaAs at low temperatures (~150 K), dissociating to form TMAA and trimethylamine (TMA) adsorbed phases as the temperature is raised.[5] This reaction scheme illustrates that TMAA and BTMAA readily dissociate on GaAs and Al surfaces below 400 K, resulting in desorption of NMe_3 into the gas phase. Although some of the free amine chemisorbs to the surface initially, blocking surface sites, desorption from the surface is rapid and complete. Thus, no film contamination results from the presence of strongly bound surface species formed by NMe_3 decomposition. This is in direct contrast to results obtained using species in which metal atoms are

* To whom correspondence should be addressed.
† Griffith University.
‡ University of New South Wales.
§ University of Queensland.
® Abstract published in *Advance ACS Abstracts*, June 15, 1994.

(1) Gladfelter, W. L.; Boyd, D. C.; Jensen, K. F. *Chem. Mater.* **1989**, *1*, 339 and references therein.
(2) Bent, B. E.; Nuzzo, R. G.; Dubois, L. H. *J. Am. Chem. Soc.* **1989**, *111*, 1634.
(3) Dubois, L. H.; Zegarski, B. R.; Kao, C. T.; Nuzzo, R. G. *Surf. Sci.* **1990**, *236*, 77.
(4) Baum, T. H.; Larson, C. E.; Jackson, R. L. *Appl. Phys. Lett.* **1989**, *55*, 1264.
(5) Wee, A. T. S.; Murrell, A. J.; Singh, N. K.; O'Hare, D.; Foord, J. S. *J. Chem. Soc., Chem. Commun.* **1990**, 11.
(6) Foord, J. S.; Murrell, A. J.; O'Hare, D.; Singh, N. K.; Wee, A. T. S.; Whitaker, T. J. *Chemtronics* **1989**, *4*, 262.
(7) Schmidt, D. L.; Hellmann, R. U.S. Patent No. 3,462,288, 1969.
(8) Daenen, T. E. G. U.K. Patent No. G.B. 2,021,646, 1979.

0897-4756/94/2806-1059$04.50/0

directly bound to carbon atoms, such as trimethylaluminum. The rate-determining step is the removal of H_2 from the surface although the ease of H_2 desorption does depend on the nature of the substrate.[6]

Techniques such as high-resolution electron energy loss spectroscopy (HREELS) and thermal desorption spectroscopy (TDS) have been used in previous studies[5,6] to investigate decomposition mechanisms and the existence of precursor and intermediate species on the surface at different temperatures. No information is obtained about film/substrate interactions and molecular orientation. X-ray photoelectron spectroscopy (XPS) and static secondary ion mass spectrometry (SSIMS) provide information which complements the techniques above. There is also the possibility of investigating adsorbate orientation and bonding to the substrate.

Herein, we report XPS and SSIMS studies of the adsorption of TMAA on oxidized silicon, which show at least two exposure-dependent adsorption processes and, for comparison, the adsorption of BTMAA on the same substrate. We also report theoretical structural and energy studies on $H_3AlNH_3(OH_2)$, as a model species for the adsorption of TMAA to surface oxygen centers, and studies of other relevant species, including H_3AlOH_2 and $H_2(NH_3)$-$Al(\mu\text{-}H)_2Al(OH_2)H_2$. These studies are also of importance in synthetic and structural chemistry of Lewis base adducts of alane; similar theoretical studies of H_3AlNH_3, $H_3Al(NH_3)_2$, and $H_2(NH_3)Al(\mu\text{-}H)_2Al(NH_3)H_2$ have already been reported.[9] Preliminary accounts of this work have been communicated previously.[10]

Experimental Section

TMAA was prepared from lithium aluminum hydride and trimethylamine hydrochloride, using a slight variation of the published procedure,[11] and purified by sublimation at 310 K. The deuterium-labeled compound $^2H_3AlNMe_3$ (TMAA-*d*) was prepared *via* the same procedure, using $LiAl^2H_4$ and $NMe_3{}^2HCl$, and was similarly purified. The isotopic purity of this compound was determined using NMR spectroscopy. BTMAA was prepared by reacting pure TMAA with an excess of TMA and used without purification.[12]

XPS experiments were carried out in ultrahigh vacuum using a Perkin-Elmer PHI 560 surface analysis system. This system contains a double-pass CMA (25–270AR) with a perpendicularly mounted dual (Mg/Mg) X-ray source operated at 500 W. Two Mg Kα X-ray sources were operated, each at 250-W. Total X-ray flux was varied between 100 and 500 W during adsorbate degradation experiments. The maximum energy resolution of the CMA was 1.2 eV operated for XPS analysis in the fixed analyzer transmission (FAT) mode with a pass energy of 25 eV for the Ag $3d_{5/2}$ emission. The electron binding energies (E_B) were calibrated against the Au $4f_{7/2}$ emission at E_B = 84 eV.[13,14]

Carbon 1s, nitrogen 1s, and aluminum 2p photoelectron peaks were fitted with a least-squares routine using Gaussian/Lorentzian peak shapes. The appropriate constraints for line shape (85% Guassian/15% Lorentzian) and fwhm for the C 1s and Al 2p photoelectron peaks were determined by analyzing chemically equivalent standards (polyethylene and Al_2O_3 on Al) under similar data acquisition conditions (pass energy 25 eV, acquisition times 20–30 min). Atomic concentrations were quantified using peak areas and empirically derived elemental sensitivity factors.[15,16] Sample charging (except C 1s photoelectron peaks, as indicated) was referenced to the Si 2p photoelectron peak from SiO_2 at 103.8 eV.[17]

XPS was used to estimate film thickness by quantifying the attenuation of a characteristic substrate peak by a thin uniform overlayer of adsorbed material. Film thickness, *d*, is given by

$$d = -\Gamma \ln[I/I_0] \quad (1)$$

where Γ is the electron mean free path in the overlayer and I and I_0 are the intensities of a characteristic peak from a covered substrate and a clean substrate, respectively. The accuracy of this technique depends on the accuracy of the electron mean free path and the uniformity of the overlayer. A nonuniform overlayer will give substrate peaks dominated by contributions from the thinnest portions of the film due to the exponential thickness/peak intensity relationship.[18]

SSIMS experiments were carried out using a Perkin-Elmer PHI 2500 SIMS I system incorporated in the surface analysis system described above. This consists of a quadrupole mass spectrometer (UTI 100C) linked with a Perkin-Elmer CMA type ion energy analyzer. SSIMS data were acquired using a 4-keV, Xe^+ primary ion beam of 5 nA rastered over 1 cm^2. A low-energy electron flood gun was used for charge neutralization. A total ion dose of 3.7×10^{12} ions cm^{-2} was delivered to the sample during a typical data acquisition.

The alane adducts were stored in a Schlenk vacuum flask and degassed at $\sim 10^{-5}$ Torr. The composition of precursors in the gas phase was monitored using a quadrupole mass spectrometer (UTI 100C) during dosing. Silicon substrates with a thermally grown oxide layer (5000 Å) were used. Substrates were washed with acetone (AR grade) and then sputter etched *in situ* using Ar^+ ion bombardment. Dosing was performed immediately after etching. Exposure was measured in langmuirs (1 langmuir = 1-s exposure at 1×10^{-6} Torr).

Ab initio calculations were performed using the Gaussian 90 package[19] on SUN SPARC Station 2 and IBM RS 6000 platforms, at the Hartree–Fock (HF) level of theory using double-zeta plus polarization (D95*) basis sets.

Results and Discussion

Substrate Characterization. The surface of the oxidized silicon substrates was prepared for adsorption by argon ion sputter etching. It has been reported that ion sputtering of thermally grown SiO_2 causes little net change in surface structure as the oxide bonds re-form after sputtering with no reduction or rearrangement, and only slight changes are observed in Si–O–Si bond angles.[20] The level of adventitious carbon on the etched substrate surface was 1–2 atom %. Sources of adventitious carbon include adsorption of contaminants and readsorption of reactive carbon species formed on the surface during sputtering. The rate of adsorption of carbon species on the substrate was monitored using XPS (Figure 1). Initially, readsorption of carbon species is quite rapid, with levels of 3 atom % attained after 30 min. Dosing experiments were carried out over a 5–15-min period after etching, in competition with the adsorption of adventitious carbon.

(9) Atwood, J. L.; Bennett, F. R.; Elms, F. M.; Jones, C.; Raston, C. L.; Robinson, K. D. *J. Am. Chem. Soc.* **1991**, *113*, 8183.
(10) Elms, F. M.; Lamb, R. N.; Pigram, P. J.; Gardiner, M. G.; Wood, B. J.; Raston, C. L. *J. Chem. Soc., Chem. Commun.* **1992**, 1423.
(11) Ruff, J. K.; Hawthorne, M. F. *J. Am. Chem. Soc.* **1960**, *82*, 2141.
(12) Heitsch, C. W.; Nordman, C. E.; Parry, R. W. *Inorg. Chem.* **1963**, *2*, 508.
(13) Bird, R. J.; Swift, T. *J. Electron Spectrosc. Relat. Phenom.* **1980**, *21*, 227.
(14) Seah, M. P. *Surf. Interface Anal.* **1989**, *14*, 488.
(15) Wagner, C. D.; Davis, L. E.; Zeller, M. V.; Taylor, J. A.; Raymond, R. H.; Gale, O. H. *Surf. Interface Anal.* **1981**, *3*, 211.
(16) Ward, R. J.; Wood, B. J. *Surf. Interface Anal.* **1992**, *18*, 679.
(17) Paparazzo, E. *Surf. Interface Anal.* **1989**, *12*, 115.
(18) Lamb, R. N.; Baxter, J.; Grunze, M.; Kong, C. W.; Unertl, W. N. *Langmuir* **1988**, *4*, 249.
(19) Frisch, M. J.; Head-Gordon, M.; Trucks, G. W.; Foresman, J. B.; Schlegel, H. B.; Raghavachari, K.; Robb, M.; Binkley, J. S.; Gonzalez, C.; Defrees, D. J.; Fox, D. J.; Whiteside, R. A.; Seeger, R.; Melius, C. F.; Baker, J.; Martin, R. L.; Kahn, L. R.; Stewart, J. J. P.; Topiol, S.; Pople, J. A. *Gaussian 90, Revision J*; Gaussian, Inc.: Pittsburgh, PA, 1990.
(20) Hofmann, S.; Thomas, III, J. H. *J. Vac. Sci. Technol. B* **1983**, *1*, 43.

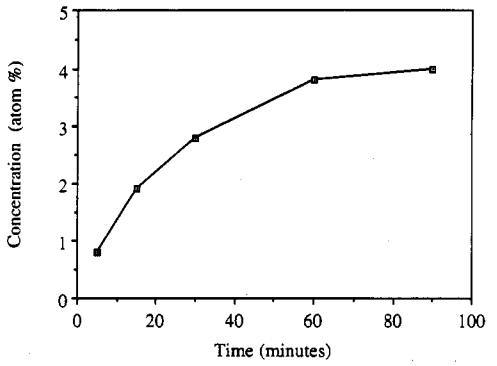

Figure 1. Rate of adsorption of adventitious carbon on a sputter-cleaned SiO_2 substrate surface deduced from changes in C 1s photoelectron peak area as a function of time.

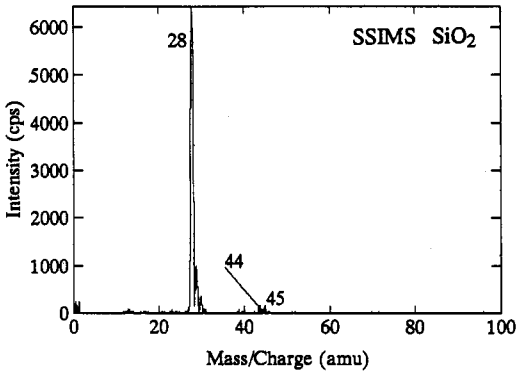

Figure 2. SSIMS spectrum for a sputter-cleaned SiO_2 substrate surface prior to dosing. Peak assignments: M^+ = 28, 29, and 30 correspond to SiH_n^+, n = 0, 1, and 2; M^+ = 45 corresponds to $SiOH^+$.

A trace of hydroxyl groups was identified using positive SSIMS ($SiOH$, M^+ = 45 Da), Figure 2. Quasi-quantitative analysis can be achieved using SSIMS by comparison of peak area ratios. The level of hydroxylation of quartz and oxidized silicon substrates can be determined by comparison of the $SiOH^+(M^+=45)/Si^+(M^+=28)$ and the $OH^-(M^+=17)/O^-(M^+=16)$ peak area ratios.[21] The surface hydroxyl levels of the oxidized silicon substrates used in this study were monitored using peak area ratios. Typical values of 45/28 = 0.016 and 17/16 = 0.05 indicate very low levels of surface hydroxyl groups (45/28 > 0.2, 17/16 > 0.2 for 100% hydroxylation).[21] The rate of rehydroxylation of the oxidized silicon surface in the vacuum chamber (base pressure 2×10^{-8} Torr) was slow. (No appreciable increase in the $SiOH^+/Si^+$ peak area ratio was observed over 1 h.)

Ion beam etching has removed organic surface contamination, as shown by the absence of $C_nH_x^+$ species. Peaks corresponding to carbon-containing species appear with time, indicating readsorption of adventitious carbon. The principal gases present in the XPS vacuum chamber (base pressure 2×10^{-8} Torr) monitored using QMS were H_2, H_2O, CO, CO_2, Ar, and Xe. No aluminum or nitrogen species were detected (using SSIMS and XPS) on the surface prior to dosing.

Adsorption of Trimethylamine–Alane (TMAA). Oxidized silicon substrates were dosed at room temperature with TMAA using a range of exposures. The composition of the presursor in the gas phase was

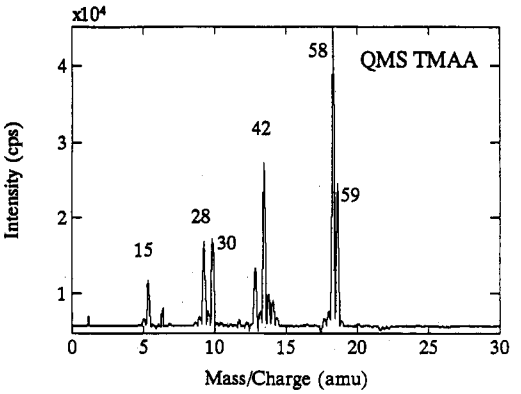

Figure 3. QMS spectrum showing the composition of the precursor in the gas phase. The ion species contributing to the principal masses shown in the spectrum most likely arise initially from fragmentation of the relatively weak Al–N bond. The peaks at 15, 42, 58, and 59 Da match CH_3^+, $N(CH_2)_2^+$, $N(CH_3)_2CH_2^+$, and $N(CH_3)_3^+$, respectively, whereas peaks at 28 and 30 Da match AlH_n^+, n = 1 and 3.

determined by subtracting the residual gas analysis of the chamber vacuum from the gas analysis performed during dosing (using the QMS); see Figure 3. The ion species contributing to the principal masses shown in the spectrum most likely arise initially from fragmentation of the relatively weak Al–N bond (see below) during analysis. (The standard electron energy of 70 eV used for recording mass spectra is much greater than the energy required to break the Al–N bond, 13.16 kcal mol^{-1}; see below.) The peaks at 15, 42, 58, and 59 Da match CH_3^+, $N(CH_2)_2^+$, $N(CH_3)_2CH_2^+$, and $N(CH_3)_3^+$, respectively, whereas peaks at 28, 29, and 30 Da match AlH_n^+, n = 1 (also matches NCH_2), 2, and 3.

Figure 4 shows the principal photoelectron peaks (carbon, nitrogen, and aluminum) for an oxidized silicon substrate dosed with 15 langmuirs of TMAA at a dose pressure of 5×10^{-8} Torr. The broad, symmetric Al 2p photoelectron peak arising from TMAA adsorption (E_B = 75.6 eV, fwhm ~ 2 eV) (Figure 5c) is consistent with Al^{III} or Al–O species.[22] This assignment was confirmed by a comparison with the Al 2p photoelectron peak shape for oxidized aluminum. Quantification of the Al 2p and N 1s photoelectron peak areas for the adsorbed material yields an Al:N ratio of ~1:1, which is consistent with the alane–amine linkage being maintained. The film thickness has been estimated to be ~2 Å, which suggests the presence of a submonolayer, discontinuous film. No changes were detected in substrate photoelectron peaks after TMAA adsorption due to low surface coverage; XPS analysis depth (~100 Å) is much greater than the effective film thickness in this instance.

Peak shape analysis of highly resolved C 1s photoelectron peaks before and after adsorption of TMAA was used to distinguish between adsorbed carbon-containing species and background adventitious carbon. The C 1s photoelectron peak for the oxidized silicon surface prior to dosing was deconvoluted into four component peaks using appropriate constraints (E_B = 285.2, 286.8, 288.25, and 289.6 eV) (Figure 5a). The C 1s peak energies are not charge corrected; charging of the oxidized silicon surface

(21) Wood, B. J.; Lamb, R. N.; Raston, C. L. *Surf. Interface Anal.*, submitted.

(22) *Handbook of X-ray Photoelectron Spectroscopy*; Perkin Elmer Corporation, Physical Electronics Division: Eden Prairie, MN, 1979.
(23) Desimoni, E.; Casella, G. I.; Cataldi, T. R. I.; Malitesta, C. *J. Electron Spectrosc. Relat. Phenom.* **1989**, *49*, 247.

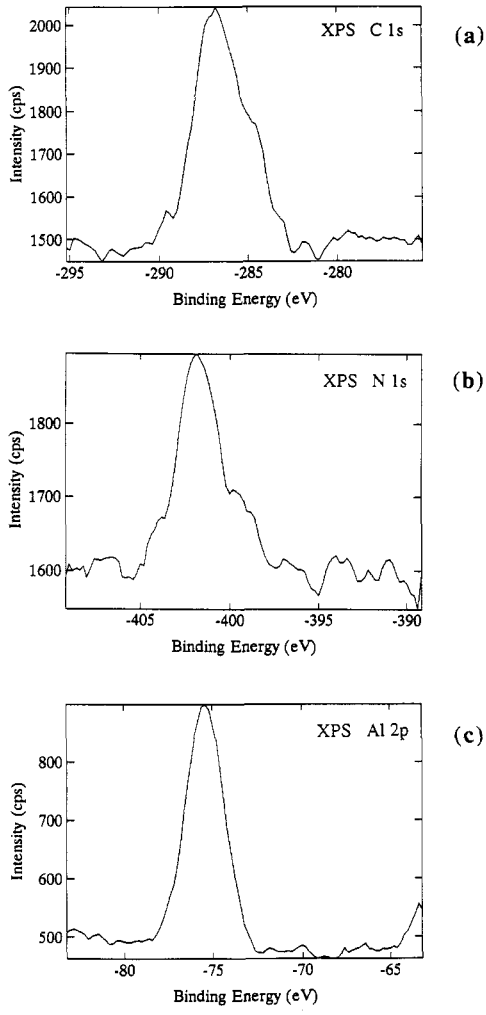

Figure 4. X-ray photoelectron spectra for TMAA adsorption on a SiO_2 surface: (a) C 1s, (b) N 1s, and (c) Al 2p. Note the multiple species character of the C 1s and N 1s spectra.

was determined to be ~3 eV. This result is consistent with the presence of carbon and oxidized carbon contaminants on the sample surface (charged, +~3 eV: carbon, E_B = 288.3 eV; oxidized carbon, E_B = 289.6 eV) and other reactive species most likely arising from carbonaceous material formed during the etching process (uncharged: carbon, E_B = 285.2 eV; oxidized carbon, E_B = 286.8 eV).[24] The C 1s photoelectron peak for the oxidized silicon substrate after dosing with TMAA (150 langmuirs) is shown in Figure 5b. The additional peak shown (E_B = 290.8 eV, no charge correction) is attributed to methyl groups from adsorbed TMAA.

The N 1s photoelectron peak arising from TMAA adsorption was deconvoluted into two component peaks (E_B = 399.2 and 402 eV) (Figure 6a). The higher binding energy component is attributed to nitrogen from molecularly adsorbed TMAA where the integrity of the alane–amine linkage (an Al–N bond) is maintained. The lower binding energy component is attributed to the adsorption of free TMA on the substrate. Binding of the amine group to electron-deficient silicon sites of surface siloxane bridges is the most likely adsorption mechanism. This assignment has been confirmed by dosing an oxidized silicon substrate

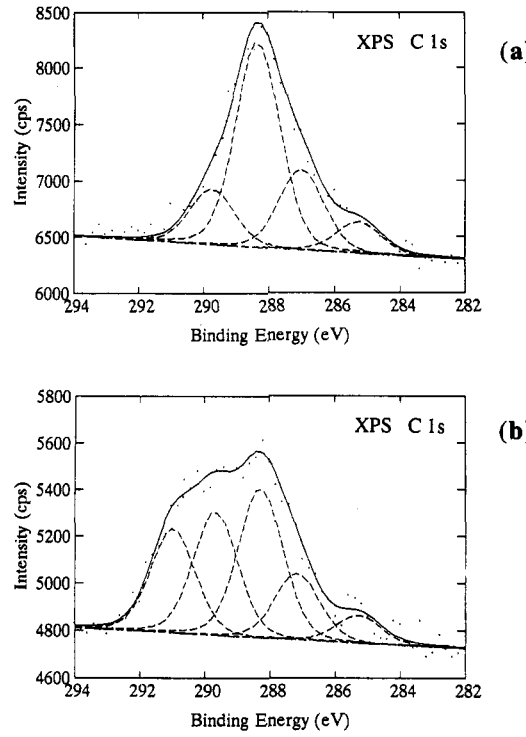

Figure 5. Curve-fitted C 1s photoelectron peaks for a sputter-cleaned SiO_2 surface: (a) before dosing and (b) after dosing with TMAA (spectra not charge corrected).

with TMA. Adsorption of TMA (30-langmuir exposure) resulted in a symmetric N 1s photoelectron peak (E_B = 399.2 eV), which was identical to the corresponding N 1s peak component resulting from TMAA adsorption (Figure 6b).

Decomposition of adsorbed TMAA is observed at high X-ray flux (>240 W), resulting in significant changes in the shape of the N 1s and C 1s photoelectron peaks. The N 1s component peak attributed to TMA substrate adsorption (399.2 eV) is significantly enhanced relative to the adsorbed TMAA peak (402 eV) (Figure 6c). The change in the peak area ratio with X-ray exposure (Figure 7) indicates an apparent release of amine by rupture of the Al–N bond followed by complexation to silicon centers on the substrate. X-ray-induced cleavage of the Al–N bond is consistent with the predicted low bond energy (see theoretical calculations in latter section) and the ability of silicon to expand its coordination sphere with electronegative centers such as nitrogen.[24] The C 1s component peak attributed to adsorbed TMAA (E_B = 290.8 eV, no charge correction) is reduced in intensity relative to other carbon species. This may result from the adsorption of TMA on the substrate and a corresponding change in the binding energy of carbon contained in adsorbed TMA methyl groups or the formation of other carbon species on the surface as byproducts of the decomposition process.

SSIMS data for TMAA adsorbed on oxidized silicon are shown in Figure 8. The spectrum is consistent with a submonolayer adsorbate film on the clean SiO_2 substrate. Because SSIMS inherently provides a mass spectrum of the outermost molecular layer,[25] it is unlikely that a surface fully covered by TMAA would exhibit $^{28}Si^+$ species in its

(24) See for example: van der Ancker, T.; Jolly, B. S.; Lappert, M. F.; Raston, C. L.; Skelton, B. W.; White, A. H. *J. Chem. Soc., Chem. Commun.* **1990**, 1006 and references therein.

(25) Briggs, D.; Brown, A.; Vickerman, J. C. *Handbook of Static Secondary Ion Mass Spectrometry*; John Wiley and Sons: New York, 1989.

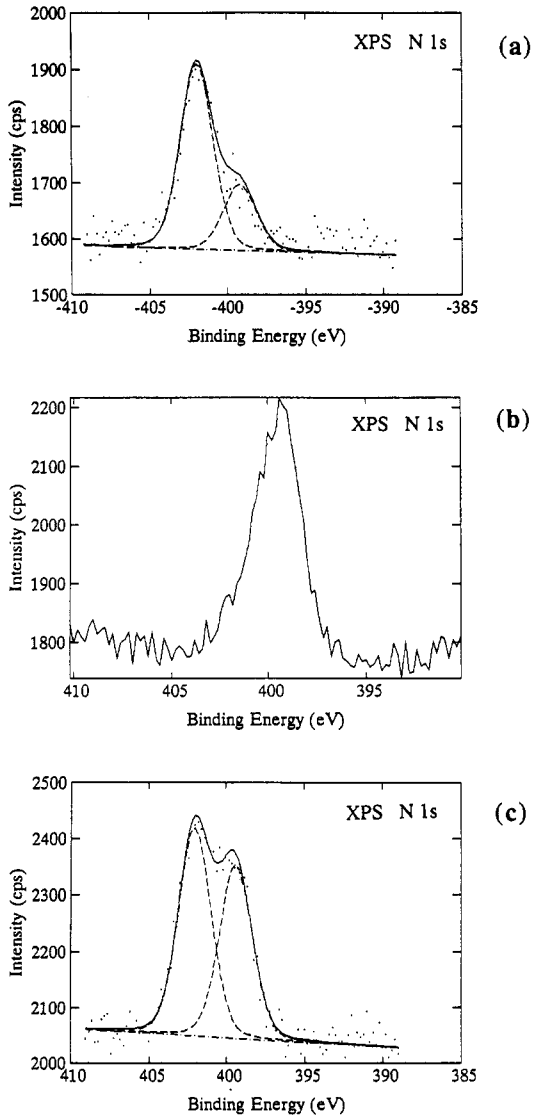

Figure 6. (a) Curve-fitted N 1s photoelectron peak for TMAA adsorption on a sputter-cleaned SiO_2 surface. (b) N 1s photoelectron peak for TMA adsorption on a sputter-cleaned SiO_2 surface. (c) Curve-fitted N 1s photoelectron peak showing X-ray-induced decomposition of the TMAA adsorbate at 500-W X-ray flux after 35-min exposure.

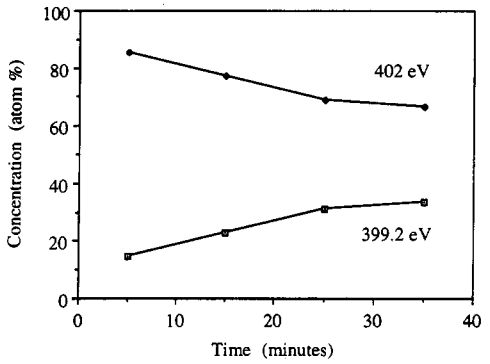

Figure 7. Rate of X-ray-induced degradation of TMAA adsorbate on a sputter-cleaned SiO_2 substrate surface deduced from changes in N 1s photoelectron component peak areas as a function of X-ray exposure.

spectrum. The ion species contributing to the principal mass species most likely arise initially from fragmentation of the relatively weak Al–N bond (see below). The peaks at 59 and 44 Da match NMe_3^+ and NMe_2^+, respectively,

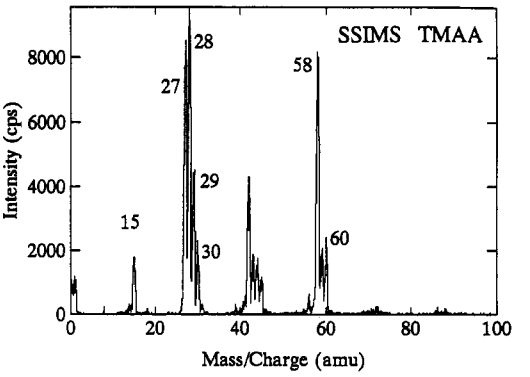

Figure 8. SSIMS spectrum for TMAA adsorbed on sputter-cleaned SiO_2 surface. Peak assignments (M^+): 15 = CH_3^+; 27 = Al; 28 = Si^+, AlH^+; 29, 30 = AlH_n^+ n = 2, 3; 58 = $N(CH_3)_2CH_2^+$; 59 = $N(CH_3)_3^+$; 60 = $HN(CH_3)_3^+$.

Scheme 1

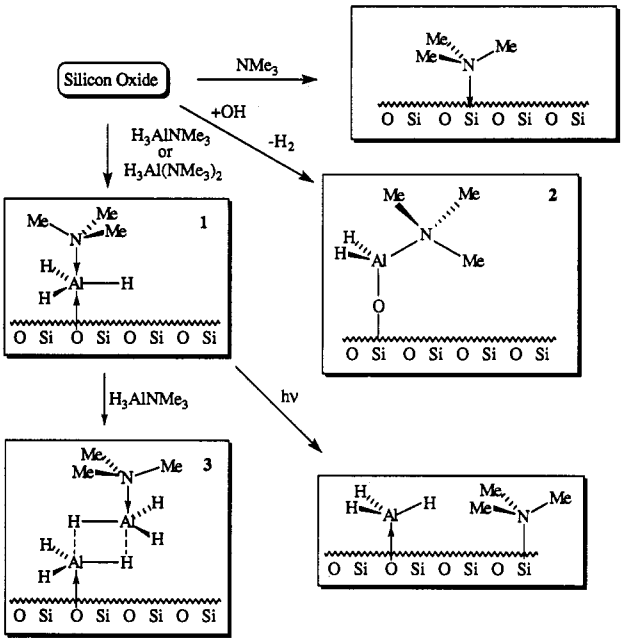

whereas peaks at 27, 28, 29, and 30 Da match AlH_n^+, n = 0, 1, 2, and 3 (1 and 2 also match $^{28}Si^+$ and $^{28}SiH^+$).

On the basis of the above data, the following model was proposed. For a surface devoid of hydroxyl groups (SiOH), the primary process for molecular adsorption of TMAA most likely involves complexation of the metal centers to oxygen atoms on the surface (Scheme 1, 1). The resulting five-coordinate aluminum species is expected to be trigonal bipyramidal with the AlH_3 unit in the trigonal plane. This is supported by (i) the theoretically determined inherent stability of the corresponding isomer for $H_3Al(NH_3)_2$ relative to that with one or two H atoms in apical positions of a trigonal bipyramid[26] and (ii) the theoretical structure of $H_3AlNH_3(OH_2)$ and associated energies. A chemical precedent for this geometry also exists in the *N*-methylmorpholine adduct of alane (ν_{Al-H} = 1745 cm^{-1}), which has a polymeric structure in the solid state with O–$Al(H)_3$–N units.[27] The Al–O interaction is weak with a bond length (2.19(2) Å) which is greater than that generally seen for dative Al–O bonds (stronger interaction).

(26) Atwood, J. L.; Bennett, F. R.; Jones, C.; Koutsantonis, G. A.; Raston, C. L.; Robinson, K. D. *J. Chem. Soc., Chem. Commun.* **1992**, 541.
(27) Atwood, J. L.; Butz, K. W.; Gardiner, M. G.; Jones, C.; Koutsantonis, G. A.; Raston, C. L.; Robinson, K. D. *Inorg. Chem.*, submitted.

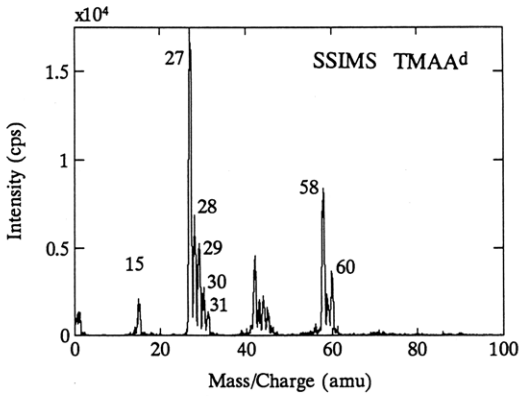

Figure 9. SSIMS spectrum for TMAA-*d* adsorbed on sputter-cleaned SiO_2 surface. Peak assignments (M^+): 15 = CH_3^+; 27 = Al^+; 28 = Si^+; 29, 31 = $Al^2H_n^+$ n = 1, 2; 58 = $N(CH_3)_2CH_2^+$; 59 = $N(CH_3)_3^+$; 60 = $HN(CH_3)_3^+$; 61 = $^2HN(CH_3)_3^+$.

In the presence of surface hydroxyls, TMAA would react to form four-coordinate species and eliminate molecular hydrogen (Scheme 1, **2**). Given the low hydroxyl levels on the surfaces used in this study (as shown by SSIMS), this would be a minor adsorption process. For higher exposures of TMAA, the Al:N ratio moves toward 2:1. Higher aluminum loading can be rationalized by ligand displacement of adsorbed species, yielding the bis(amine) adduct BTMAA in the vapor phase and a hydride-bridged species on the surface (Scheme 1, **3**) of the type identified for a range of monoamine adducts of alane in the solid state.[9] See below for calculated energy and structural aspects of this model.

Simmonds *et al.* have performed studies using FTIR on the surface chemistry of dimethylethylamine–alane (DMEAA) on a hydroxylated silicon oxide surface.[28] They observed weakly bound molecular DMEAA (ν_{Al-H} = 1780 cm^{-1}) analogous to the five-coordinate species proposed above for a surface devoid of hydroxyl groups (Scheme 1, **1**). They also found DMEAA chemisorbed onto the surface as partially oxidized aluminum hydrides (ν_{Al-H} = 1850 cm^{-1}), bound to Si–O sites originally present as surface hydroxyl groups. Over time, these hydride species were consumed, through further reaction with water, siloxane bridges, or hydroxyl groups on the surface, resulting in loss of the amine ligand.[28] We found that TMAA dosing experiments where the oxidized silicon surfaces showed high levels of hydroxyl groups ($SiOH^+/Si^+ > 0.2$) resulted in large Al:N ratios (>4:1). The SSIMS spectrum of TMAA-*d* adsorbed onto a heavily hydroxylated surface is shown in Figure 9. The greatest deuterium-containing fragment corresponds to $Al^2H_2^+$ species (31 Da), indicating that some deuterium atoms attached to aluminum have undergone isotopic exchange and reaction with surface hydroxyl species after adsorption of the TMAA-*d* on the substrate. Overall, our results complement those recently recorded by Simmonds *et al.*

Adsorption of Bis(trimethylamine)–Alane (BTMAA). Dosing experiments using BTMAA, under analogous conditions, gave similar results to the experiments using TMAA, *viz.*, the submonolayer presence of TMAA on the surface with the integrity of the amine–alane linkage being maintained. This is consistent with dissociative adsorption of BTMAA such that the principal adsorbed species are TMAA and TMA. Molecular adsorption of BTMAA would require six-coordinate aluminum species and is not expected on steric grounds.

The binding of free amine to the surface does not appear to be a competing/concurrent process as indicated by the Al:N ratio of 1:1. Experiments where the surface was dosed with TMAA prior to dosing with TMA resulted in no change to the adsorbed TMAA species. No increase in the intensity of the lower binding energy N 1s photoelectron peak was observed. This indicates that the preadsorbed TMAA occupies and/or successfully conceals all the possible binding sites for free amine, *viz.*, the electropositive silicon of siloxane bridges. X-ray degradation of the adsorbed BTMAA species was also observed as changes in the line shape of the N 1s photoelectron peak with increasing X-ray exposure.

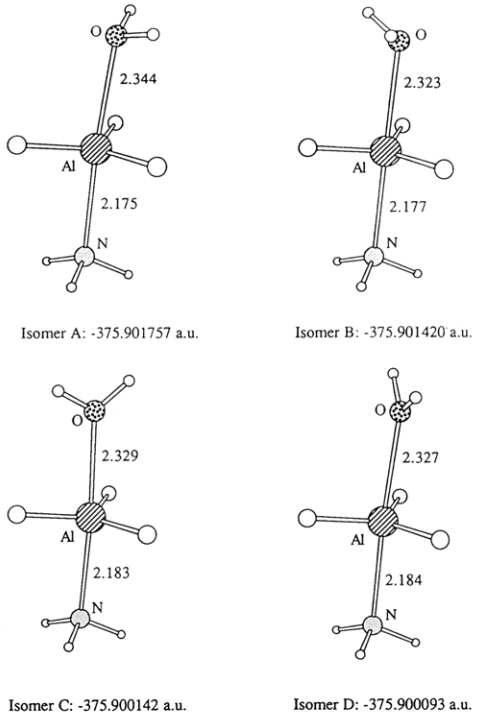

Figure 10. Optimized structures for $H_3AlNH_3(OH_2)$ (C_s symmetry).

***Ab Initio* Molecular Orbital Calculations.** Theoretical calculations were undertaken to investigate the feasibility of the adsorption model outlined in Scheme 1. It has been assumed that adsorption occurs on a model SiO_2 substrate. While the SiO_2 substrates prepared for adsorption experiments have a more complicated surface structure, XPS and SSIMS results indicate the existence of well-defined modes of precursor adsorption and degradation. The adsorption model proposed is consistent with experimental results and is intended as a best approximation of adsorption behavior.

Theoretical calculations on the model compound for surface adsorption, $H_3Al(NH_3)(OH_2)$, at the HF/D95* level converged on four isomers with imposed C_s symmetry (Figure 10) with energies within 1.04 kcal mol^{-1}. Removing the symmetry constraint resulted in convergence on the same structures. Computed energies and geometries for C_s symmetry are shown in Table 1. There are two pairs of isomers, one with sp^3 O-centers (A and B) and the other with sp^2 O-centers (C and D), and the difference within each pair is the orientation of the O-centered H atoms. Isomer A was shown to be a minimum by frequency analysis whereas isomers B and C were transition states of order

(28) Simmonds, M. G.; Zazzera, L. A.; Evans, J. F.; Gladfelter, W. L. *Chem. Mater.*, in press.

Table 1. Optimized Energies and Geometries for H_3AlOH_2 and $H_3AlNH_3(OH_2)$[a]

	H_3AlOH_2[b]				$H_3AlNH_3(OH_2)$[b]			
	A	B	C	D	A	B	C	D
energy	-319.681693	-319.681592	-319.681241	-319.681203	-375.901757	-375.901420	-375.900142	-375.900093
Al-O	2.067	2.062	2.059	2.059	2.344	2.323	2.329	2.327
Al-N					2.175	2.177	2.183	2.184
Al-H(1)	1.590	1.598	1.596	1.593	1.600	1.613	1.610	1.606
Al-H(2)	1.597	1.593	1.593	1.594	1.612	1.605	1.606	1.608
O-H(3)	0.951	0.951	0.950	0.950	0.949	0.949	0.948	0.948
O-H(4)			0.950				0.948	
N-H(5)					1.005	1.006	1.005	1.005
N-H(6)					1.006	1.005	1.005	1.005
O-Al-N					175.9	179.5	176.1	176.8
H(1)-Al-H(2)	117.9	117.1	118.5	117.3	120.1	118.4	120.4	119.0
O-Al-H(1)	102.3	99.3	94.6	101.3	91.2	87.6	83.6	90.6
O-Al-H(2)	96.0	97.5	100.1	96.7	85.1	87.0	89.3	85.9
Al-O-H(3)	117.7	118.9	122.6	124.8	109.1	111.6	121.2	125.3
Al-O-H(4)			127.0				129.4	
H-O-H	109.0	109.0	110.4	110.4	107.5	107.4	109.3	109.3
Al-N-H(5)					111.6	111.0	110.7	111.4
Al-N-H(6)					110.9	111.1	111.2	110.9
H(1)-Al-O-H(2)	120.4	119.1	120.0	119.6	120.4	118.6	120.6	119.2
H(1)-Al-O-H(3)	113.1	68.3	0.0	90.1	121.4	60.1	0.0	90.1
H(1)-Al-O-H(4)			180.0				180.0	
H(1)-Al-N-H(6)					59.8	60.1	60.1	60.0

[a] Energy is in hartrees, bond lengths are in angstroms, and bond angles are in degrees. [b] Refer to Figures 10 and 11 for atom labeling and isomer identification. Geometry of H_2O (C_{2v}, -76.035 155 hartrees): O-H, 0.947 Å; H-O-H, 106.4°. Geometry of NH_3 (C_{3v}, -56.199 090 hartrees): N-H, 1.004 Å; H-N-H, 107.7°. Geometry of H_3AlNH_3 (C_{3v}, -299.859 374 hartrees): Al-H, 1.600 Å; Al-N, 2.095 Å; N-H, 1.007 Å; H-N-Al, 111.4°; H-Al-N, 99.5°.

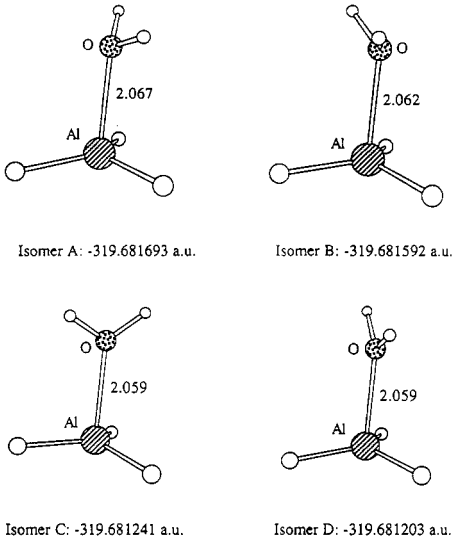

Figure 11. Optimized structures for H_3AlOH_2 (C_s symmetry).

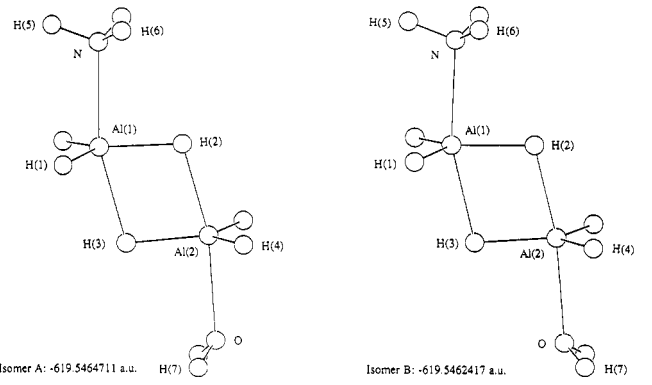

Figure 12. Optimized structures for $H_2(H_3N)Al(\mu\text{-}H)_2Al(OH_2)\text{-}H_2$ (C_s symmetry). Important bond lengths and bond angles of isomers A and B, respectively: Al(1)-N 2.160, 2.161; Al(2)-O 2.193, 2.206; Al(1)-H(1) 1.593, 1.592; Al(1)-H(2) 1.665, 1.667; Al(1)-H(3) 2.032, 2.038; Al(2)-H(2) 1.933, 1.939; Al(2)-H(3) 1.653, 1.640; Al(2)-H(4) 1.588, 1.503; N-H(5) 1.006, 1.006; N-H(6) 1.006, 1.006; O-H(7) 0.950, 0.950; N-Al(1)-H(3) 165.0, 164.9; H(2)-Al(2)-O 168.1, 171.2; N-Al(1)-H(1) 94.4, 94.3; N-Al(1)-H(2) 88.1, 88.1; H(1)-Al(1)-H(3)-, 92.6; H(2)-Al(1)-H(3) 76.9, 76.8; Al(1)-H(3)-Al(2) 99.9, 99.6; H(2)-Al(2)-H(3) 79.9, 80.6; H(2)-Al(2)-H(4) 94.9, 94.9; H(4)-Al(2)-O 90.4, 89.2; Al(2)-O-H(7) 116.0, 114.85; H(7)-O-H(7)′ 108.2, 108.4; H(5)-N-Al(1) 111.6, 110.7; H(6)-N-Al(1) 111.4, 111.5.

1, and isomer D was a transition state of order 2. The stabilization energy of $H_3AlNH_3(OH_2)$ relative to H_3AlNH_3 and OH_2 is 4.71 kcal mol^{-1} (isomer A), which is consistent with the binding of TMAA to surface oxygen centers of SiO_2. Calculations on H_3AlOH_2 as a model for the species derived from X-ray-induced loss of NMe_3 converged similarly on four isomers (Figure 11), in pairs, with similar differences in orientation of the O-centered H atoms; energies and geometries are given in Table 1. As for the mixed donor calculation isomer A was a true minimum, whereas B–D were transition states of the same order. Conversion of $H_3Al(NH_3)(OH_2)$, isomer A, to H_3AlOH_2, isomer A, and free amine requires 13.16 kcal mol^{-1}. This is a relatively low energy process and would be feasible under exposure to high X-ray flux.

The secondary adsorption process ascribed to formation of BTMAA and O-surface bound AlH_3 followed by uptake of H_3AlNMe_3 to yield bridging hydride species has also been investigated using computational chemistry, again on the appropriate model compounds. This yields $H_3Al(NH_3)(OH_2)$ and H_3AlNH_3 energetically favored relative to $H_3Al(NH_3)_2$ and H_3AlOH_2 by only 4.15 kcal mol^{-1}. Thus, at the higher dosing pressure where there is greater chance of molecular encounter of TMAA with adsorbed TMAA, dissociation of BTMAA yielding surface bound "$H_3Al{\leftarrow}O=$" is possible (eq 5). Association of such species with TMAA *via* hydride bridges, of the type found in the solid for TMAA,[9] is then possible (eq 6). Indeed, *ab initio* calculations for association of H_3AlOH_2 and H_3AlNH_3 yield formation of the hydride bridged species $H_2(NH_3)Al(\mu\text{-}H)_2Al(OH_2)H_2$ as energetically favored by 3.39 and 3.24 kcal mol^{-1} for two bridging isomers, A and B (Figure 12), both of C_s symmetry, differing in the orientation of H

atoms on sp^3 O centers. Overall, the two-step process proposed in eqs 5 and 6 is disfavored by only 0.76 and 0.91 kcal mol^{-1} for isomers A and B, respectively.

$$TMAA(g) + H_3(Me_3N)Al{\leftarrow}O{=} \rightleftharpoons BTMAA(g) + H_3Al{\leftarrow}O{=} \quad (5)$$

$$TMAA(g) + H_3Al{\leftarrow}O{=} \rightleftharpoons H_2(Me_3N)Al(\mu\text{-}H)_2AlH_2{\leftarrow}O{=}(H_2) \quad (6)$$

Summary

The dosing of TMAA on thermally grown silicon oxide results in molecular adsorption. Using XPS and SSIMS techniques, coupled with the use of deuterium-labeled species, it has been possible to derive a model for adsorption at low and higher exposures. In addition, *ab initio* structural and energy calculations are consistent with (i) molecular adsorption of TMAA on oxidized silicon with the expansion of the aluminum coordination environment, (ii) the relative ease of cleavage of the associated Al–N linkage, and (iii) the formation of the aluminum rich species at higher exposures.

Acknowledgment. The authors acknowledge the Australian Research Council for financial support of this work and IBM Australia for the provision of RS 6000 computing facilities.